Available online at www.sciencedirect.com
SCIENCE DIRECT®
Optics & Laser Technology 38 (2006) 506–511
Optics & Laser Technology
www.elsevier.com/locate/optlastec

Speckle correlation fringes denoising using stationary wavelet transform. Application in the wavelet phase evaluation technique

E.M. Barj[a,*], M. Afifi[a], A.A. Idrissi[a], K. Nassim[b], S. Rachafi[b]

[a]*Laboratoire d'optique appliquée et du traitement des images, Faculté des Sciences Ben M'sik, B.P. 7955, Sidi Othman, Casablanca, Morocco*
[b]*Faculté des Sciences El Jadida, B.P. 20, El Jadida 24000, Morocco*

Received 4 August 2004; received in revised form 1 December 2004; accepted 8 December 2004
Available online 2 March 2005

Abstract

This paper presents a stationary wavelet transform (SWT) method for speckle noise reduction in digital speckle pattern interferometry fringes. The main advantage of SWT is its translation invariance, which makes it important in statistical image processing applications. This method was used to denoise a simulated speckle fringe patterns, a good fidelity value was obtained. Applied to the wavelet phase evaluation, it has provided a phase distribution with a good accuracy.

Keywords: Wavelet transform; Denoising; Speckle interferometry; Phase retrieval

1. Introduction

Digital speckle pattern interferometry (DSPI) is a whole field optical method for non-contact and non-destructive surface analysis. It's now considered as a powerful tool for industrial measurements. It enables full-field measurement of optical phase changes via the acquisition of speckle patterns [1,2]. After acquisition, a simple subtraction is usually performed to obtain a fringe pattern.

The greatest challenges in speckle interferometry focus on relating fringe patterns to phase mapping, permitting the direct determination of surface deformation. However, as DSPI fringes are characterized by a strong speckle noise background, a denoising method must be used before the phase evaluation.

Wavelet techniques have become an attractive and efficient tool in image denoising. A fast algorithm of discrete wavelet transform (DWT) is multiresolution analysis [3], which is a non-redundant decomposition. The drawback of non-redundant transform is their non-invariance in space, i.e. the coefficients of a delayed signal are not a space-shifted version those of the original signal. A new algorithm was introduced in [4] known as stationary wavelet transform (SWT) that makes the wavelet decomposition space invariant. This improves the power of wavelet in image denoising. In this paper we are going to use the SWT (method) to denoise a simulated speckle fringe pattern and apply it in the wavelet phase extraction technique [5].

2. Computer simulated DSPI fringes

In order to generate the speckle patterns diffracted by a surface, we simulate the clean imaging optical system [6] shown in the Fig. 1 to generate fringe patterns as in an out of plane interferometer.

Within the paraxial approximation, optical propagation through any complex optical system, described by an ABCD ray transfer matrix, can be formulated by Collins formulas [7]. Collins has obtained an analytic form for the resulting complex field amplitude. Let $U(x_0, y_0)$ be the field on the input plane (x_0, y_0) located at $z = 0$. The diffraction integral relating the fields

*Corresponding author.
E-mail address: mu_barj@hotmail.com (E.M. Barj).

0030-3992/$ - see front matter © 2005 Elsevier Ltd. All rights reserved.
doi:10.1016/j.optlastec.2004.12.007

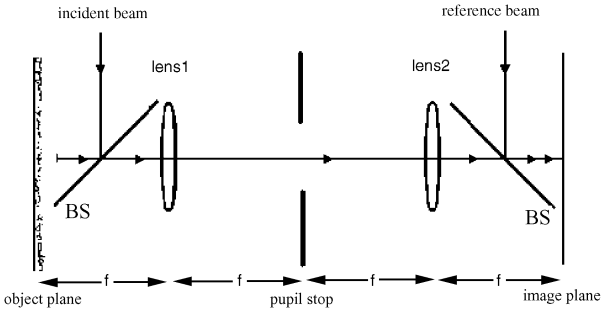

Fig. 1. Schematic setup.

across the input and output planes can be expressed as

$$U(x,y) = \frac{j}{\lambda B}\exp(-jkL)\iint U(x_0,y_0)\exp\left[-\frac{jk}{2B}(D(x^2+y^2) - 2(xx_0+yy_0)+A(x_0^2+y_0^2))\right]\mathrm{d}x_0\,\mathrm{d}y_0, \quad (1)$$

where (x,y) are transverse coordinates of the output plane, k is the optical wave number, j is a complex defined by $j^2=-1$, λ is the free-space wavelength, L is the optical distance along the z-axis, and A, B, D [8] are the ray matrix elements for the complete optical system between input and output planes. When the input and output planes are in free space, the determinant of $ABCD$ matrix is unity (i.e. $AD-BC=1$).

To generate a speckle pattern, the reflected field $U(x_0,y_0)$ is supposed to be given by

$$U(x_0,y_0) = r_0 P(x_0,y_0)\exp[\mathrm{i}h(x_0,y_0)], \quad (2)$$

where r_0 is the average reflectivity, P is the incident beam on the surface, and h is a random phase uniformly distributed in the interval $[-\pi,\pi]$.

In this study we apply Eq. (1) to find the field at the plane of the limiting aperture with $A=0$, $B=f$, $C=-1/f$, *et* $D=0$, multiplying it by the aperture function and applying Eq. (1) a second time to the remainder of the system with $A=0$, $B=f$, $C=-1/f$, and $D=0$.

By varying the limiting aperture radius, we can match the target resolution to ensure a fully resolved speckle pattern across the observation plane.

Out-of-plane DSPI interferometers combine the optical field scattered by the object with a uniform reference field. The first order statistics of the interference of a speckle pattern and a reference field with zero phase are given by the equation [9]

$$\rho(I) = \frac{\exp[-(I+I_\mathrm{r})/\langle I\rangle]}{\langle I\rangle} I_0\left(2\frac{(II_\mathrm{r})^{1/2}}{\langle I\rangle}\right), \quad (3)$$

where I_0 is the zero-order first kind modified Bessel function, $\langle I\rangle$ is the intensity average of the speckle field alone, and I_r is the intensity of the reference field with zero phase, such that the beam ratio $r = I_\mathrm{r}\langle I\rangle^{-1}$.

Several interferograms with various speckle sizes were evaluated. In all the cases we have found a good agreement between the numerical model and the theoretical curve of the probability density function given by Eq. (3). Fig. 2 shows such a comparison for an interferogram with an average speckle size of three pixels when the incident beam waist was much larger than the width of the pupil stop. The speckle fringe patterns are obtained by subtraction of a reference speckled image from image of displaced surface.

The intensity distribution of a reference speckled image (before displacement) is

$$I_1(x,y) = I_\mathrm{b}(x,y)[1+V(x,y)\cos(\phi_\mathrm{s}(x,y))], \quad (4)$$

where I_b is the bias intensity, V the visibility and ϕ_s is the original phase from the speckle that appears as the high frequency and apparently random pixel-by-pixel intensity variation.

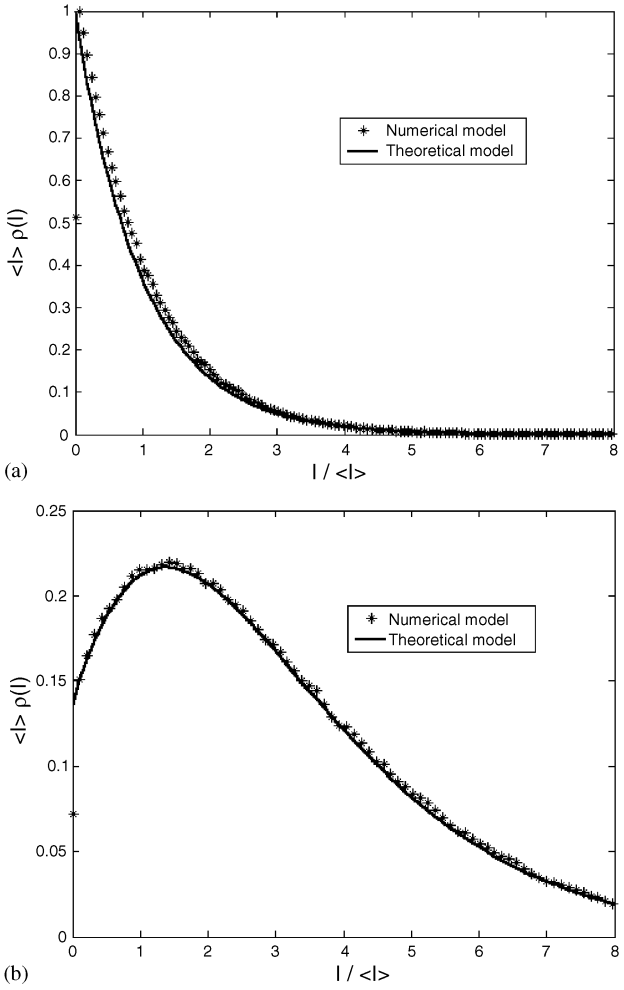

Fig. 2. Comparison between the numerical model and the theoretical curve for the probability density function of the intensity, in (a) speckle field alone and in (b) speckle field with the addition of a constant reference field with zero phase with $r=2$. The average speckle size is 3 pixels.

After displacement, the intensity distribution becomes

$$I_2(x,y) = I_b(x,y)[1 + V(x,y)\cos(\phi_s(x,y) + \varphi(x,y))], \tag{5}$$

where φ is the phase change in the light resulting from the displacement. We assume that the displacements are sufficiently small that speckle decorrelation effects can be ignored.

The intensity distribution in the speckle correlogram is given by

$$I(x,y) = 2I_b V \sin\left(\frac{\varphi}{2}\right)\sin\left(\phi_s + \frac{\varphi}{2}\right). \tag{6}$$

Fringes obtained in Eq. (6) are characterized by a speckle noise background; a noise reduction method must be used before the phase distribution is evaluated.

The desired information containing the $\sin(\varphi/2)$ fringe term (shape of envelope modulating the random speckle term) may be rectified and filtered by appropriate computer image processing in order to remove the high frequency $\sin(\phi_s + \varphi/2)$ noise.

3. Wavelet analysis for optical interferometry

In optical interferometry, many research works [10–21] have developed wavelet analysis to improve metrology based on speckle interferometry in two principles domains: the fringe patterns denoising, and the phase or the local frequency extraction from the processed images.

3.1. Denoising technique

3.1.1. Discrete wavelet transform

Several texts address the principles of wavelet transform [22–24]. However, a brief description of the method is given here for completeness. The standard discrete wavelet transform DWT [3] is based on a low pass filter H and a high pass filter G and on a binary decimation.

Let $\{h_n\}$ and $\{g_n\}$ be the sequences defining the filters H and G. The filter H is assumed to satisfy the internal orthogonality relation

$$\sum_n h_n h_{n+2j} = 0 \tag{7}$$

for all integers $j \neq 0$, and to have $\sum h_n^2 = 1$. The filter G is defined by

$$g_n = (-1)^n h_{1-n} \tag{8}$$

for all n, and satisfy the same internal orthogonality as H. The filters obey the mutual orthogonality relation

$$\sum_n h_n g_{n+2j} = 0 \tag{9}$$

for all integers j. Filters constructed in this way are called quadrature mirror filters.

The binary decimation operator D_o simply chooses every even member of a sequence, so that $(D_o x)_j = x_{2j}$, for all integers j. It follows from the internal and mutual orthogonality properties of the quadrature mirror filters that the mapping of a sequence x to the mapping of sequencies $(D_o Gx, D_o Hx)$ is an orthogonal transformation. If x is a finite sequence of length 2^m with periodic boundary conditions applied, then each of $D_o Gx$ and $D_o Hx$ will be sequences of length 2^{m-1}. The discrete wavelet transform algorithm is derived from a multiresolution analysis, performed as follows. Defining the smooth c^j at level j and the detail d^j at level j by

$$c^j = D_o H c^{j+1} \quad \text{and} \quad d^j = D_o G c^{j+1}. \tag{10}$$

It can be seen from Eq. (9) that the approximation at each level is fed down to the next level to give rise to smooth and detail at that level. Because the mapping $(D_o Gx, D_o Hx)$ is an orthogonal transform, it can be easily inverted to find c^{j+1} in terms of c^j and d^j.

$$c^{j+1} = R_0(c^j, d^j), \tag{11}$$

where R_0 is the inverse transform.

The discrete wavelet transform is obtained by continuing this process to obtain the detail at each level with the approximation at the zero level. Eq. (10) shows that the process can be reversed by reconstructing c^1 from d^0 and c^0, and c^2 from d^1 and c^1, and so on.

3.1.2. Stationary wavelet transform

The standard DWT is non-redundant, which is space variant. SWT was presented in [4] and is space invariant. A clear description and analysis of the method is presented in [25]. In summary, the SWT method can at each level, after applying the low and high pass filters to the data be described as new sequences that have the same length as the original sequences. To do this, the original data is not decimated; however the filters at each level are modified by padding them out with zeros.

Let Z be the operator that alternates a given sequence with zeros, so that for all integers j, $(Z_x)_{2j} = x_j$ and $(Z_x)_{2j+1} = 0$. Define filters $H^{[r]}$ and $G^{[r]}$ to have weights $Z^r h$ and $Z^r g$, respectively. Thus the filter $H^{[r]}$ has the weight $h^{[r]}_{2^r j} = h_j$ and $h^{[r]}_{kj} = 0$ if k is not a multiple of 2^r. The filter $H^{[r]}$ is obtained by inserting a zero between every adjacent pair of elements of the filter $H^{[r-1]}$, and similarly for $G^{[r]}$. It is immediate that

$$D_0^r H^{[r]} = H D_0^r \quad \text{and} \quad D_0^r G^{[r]} = G D_0^r. \tag{12}$$

To define the stationary wavelet transform, we start by setting a^J to be the original sequence c^J. For $j = J, J-1, \ldots, 1$, we then recursively define

$$a^{j-1} = H^{[J-j]} a^j \quad \text{and} \quad b^{j-1} = G^{[J-j]} a^j. \tag{13}$$

If the vector a^J is of length 2^J, then all the vectors a^j and b^j will be of the same length, rather than becoming shorter as j decreases as in the standard DWT.

3.1.3. Denoising technique

After the SWT decomposition, the image is denoised by shrinking the coefficients from the detail subbands with a soft threshold function [26]. The procedure removes noise by thresholding only the wavelet coefficients of the detail subbands, while keeping the low-resolution coefficients unaltered. The soft thresholding rule is normally chosen, because it has been shown to achieve near-optimal minimax rate, and the optimal soft thresholding estimator yields a smaller risk than the optimal hard thresholding estimator. The threshold is generally estimated from the knowledge of the noise variance. The optimal threshold is the universal one [26] that can be estimated by means of the variance σ^2 of the coefficients in the highest level of the wavelet basis decomposition.

To evaluate the performance of the denoising method, we have calculated the fidelity f [9] defined by

$$f = 1 - \frac{\sum_1^N (I - I_{\text{ideal}})^2}{I_{\text{ideal}}^2}, \tag{14}$$

where I_{ideal} is the noiseless image and I the denoised one. The fidelity quantifies how well image details are preserved. A fidelity value close to 1 will indicate that the filtered image is similar to the noiseless one.

3.2. Wavelet phase extraction

When a high frequency spatial carrier is added to the phase, the fringe pattern of Eq. (6), leads after processing to a modulated fringe pattern which can be represented as follows

$$I(x,y) = A(x,y) + B(x,y)\cos(my + \phi(x,y)), \tag{15}$$

where $I(x,y)$, $A(x,y)$, $B(x,y)$ are recorded intensity, background intensity and fringe amplitude, respectively, $\phi(x,y)$ is the desired phase information and my is the phase modulated carrier. This spatial carrier must respect the following condition:

$$m > \left|\frac{\partial\phi}{\partial y}\right|_{\max}. \tag{16}$$

The one-dimensional wavelet transform of the fringe pattern intensity, in the y direction, is given by

$$W(x,s,\xi) = \frac{1}{\sqrt{s}}\int_{-\infty}^{+\infty} [A(x,y) + B(x,y) \times \cos(my + \phi(x,\xi))]\left(\Psi\left(\frac{y-\xi}{s}\right)\right)^* \mathrm{d}y. \tag{17}$$

Exploiting the localization property of the wavelet, the development of the phase of interest ϕ on Taylor series near the central value ξ, allowed us to write

$$\phi(x,y) = \phi(x,\xi) + (y-\xi)\frac{\partial\phi}{\partial y}(x,\xi) + \dots . \tag{18}$$

Assuming a slow variation of A and B, which is convenient in usual cases, and owing the localization of the wavelet, we can neglect the higher order of $(y-\xi)$ with respect to the phase-modulated carrier. With these considerations, the wavelet transform becomes

$$W(x,s,\xi) = \frac{B(x,\xi)}{\sqrt{s}}\int_{-\infty}^{+\infty} \cos\left[my + \phi(x,\xi) + (y-\xi)\frac{\partial\phi}{\partial y}(x,\xi)\right]\left(\Psi\left(\frac{y-\xi}{s}\right)\right)^* \mathrm{d}y. \tag{19}$$

Using an analytic wavelet, in our case Paul wavelet defined by

$$\Psi(x) = \frac{2^n n!(1-\mathrm{i}x)^{-(n+1)}}{2\pi\sqrt{(2n)!/2}} \tag{20}$$

the extremum of the scale S obtained from the modulus $|W(x,s,\xi)|$ is given by

$$S(x,\xi) = \frac{2n+1}{2m_1}, \tag{21}$$

where

$$m_1 = m + \frac{\partial\phi}{\partial y}(x,\xi). \tag{22}$$

Eqs. (21) and (22) give then the phase gradient by

$$\frac{\partial\phi}{\partial y}(x,\xi) = \frac{2n+1}{2S(x,\xi)} - m. \tag{23}$$

This leads to the phase by integration of the gradient.

4. Results of simulation

To analyze the performance of the SWT denoising technique, two fringe patterns were generated. The fringe pattern shown in Fig. 3a, obtained by adding a known phase $\phi(x_0,y_0)$ to the random phase $h(x_0,y_0)$ such that

$$\phi(x_0,y_0) = 0.0004((x-256)^2 + (y-256)^2) \tag{24}$$

and the high frequency modulated fringe pattern shown in Fig. 3b, obtained by adding a high frequency spatial carrier my to the phase, with $m = 0.63$ radian/pixel. The fringe patterns are obtained for an average speckle size of 3 pixels. A comparison with the DWT subband removal technique [19] is done.

In Fig. 4, we present the filtered images of the fringe pattern shown in Fig. 3a, obtained with the two methods. The upper part is obtained with the DWT method, using a Daubachies wavelet with four-length filter, keeping the LL, HL, and LH subbands in the fourth level of the wavelet decomposition and setting the

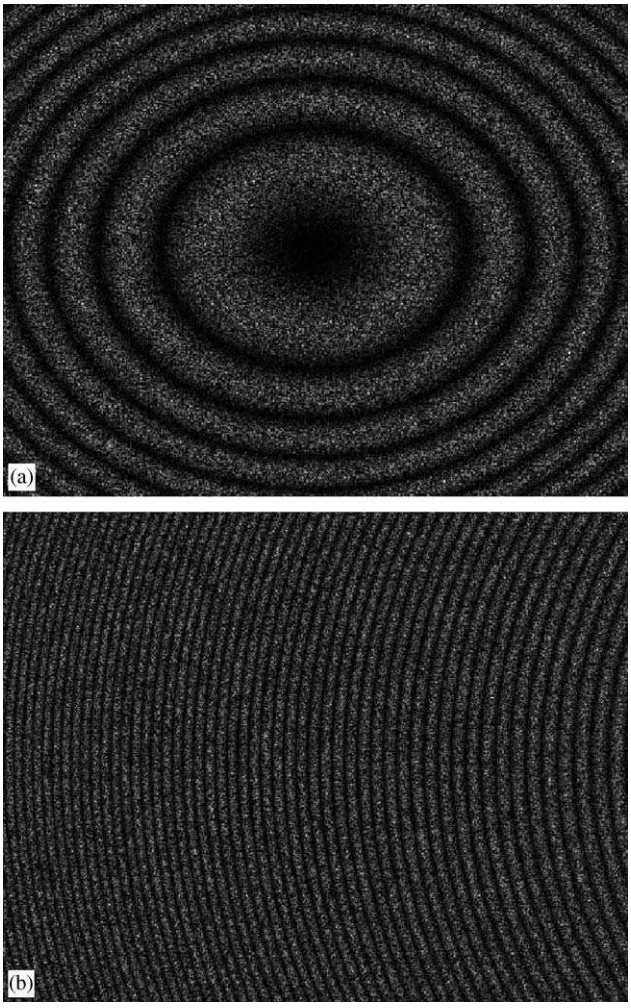

Fig. 3. (a) The noisily fringe pattern for an average size of three pixels obtained by means of the numerical model, (b) the corresponding high frequency modulated fringe pattern.

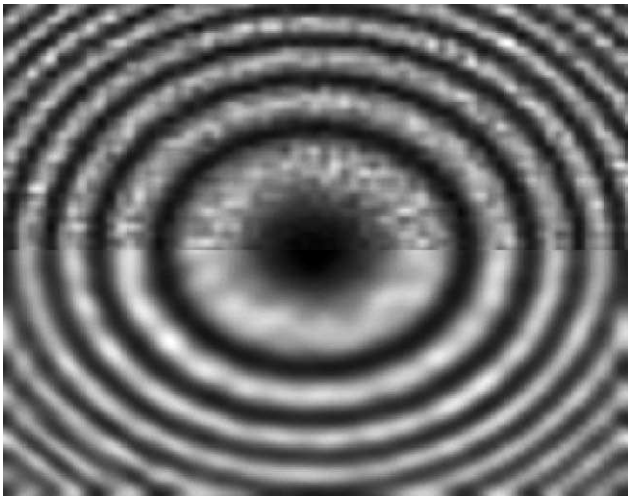

Fig. 4. The filtered fringe pattern. The upper part is the resultant one by the DWT method and the lower part is the resultant one by SWT method.

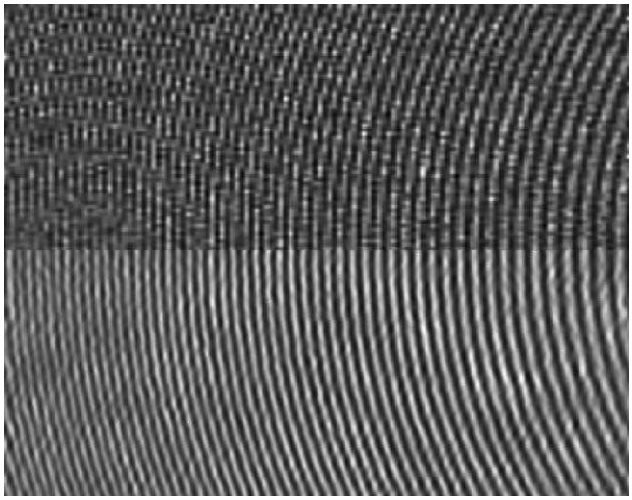

Fig. 5. The filtered high frequency modulated fringe pattern. The upper part is the resultant one by the DWT method when the image is decomposed at level 3 and the lower part is the resultant one by SWT method when the image is decomposed at level 4.

other subbands to zero. The lower part is obtained with the SWT method, after the image is decomposed at level four, using the same wavelet. We have obtained a fidelity value f of 0.90 for DWT and 0.94 for the SWT technique.

The efficiency of the SWT method is shown when filtering the high frequency modulated fringe pattern of Fig. 3b. We can see in Fig. 5, upper part, that DWT method destroys the fringes when the image is decomposed at level 3 while the SWT method, in the lower part, give a good result and keep the fringes unaltered at level 4. We have obtained a fidelity value f of 0.74 for DWT and 0.87 for the SWT technique.

The wavelet phase extraction technique is then applied to the SWT filtered modulated fringe pattern, lower part of the Fig. 5, to retrieve the phase distribution. The recovered phase distribution is presented in Fig. 6a, and the exact phase of Eq. (24) is shown in Fig. 6b; using the fidelity coefficient for comparison, we have obtained a fidelity value of 0.9916. Fig. 6c shows the difference between the two phase distributions represented by a gray scale levels. Over the majority of the surface, the two distributions are in a good agreement.

5. Conclusion

In this paper the SWT method is used to reduce speckle noise in DSPI fringes. The study is carried out in computer simulated fringes through the evaluation of the fidelity parameter. It is shown that the SWT method is appropriate to remove the speckle noise and maintains the fringe pattern features especially for fringe patterns

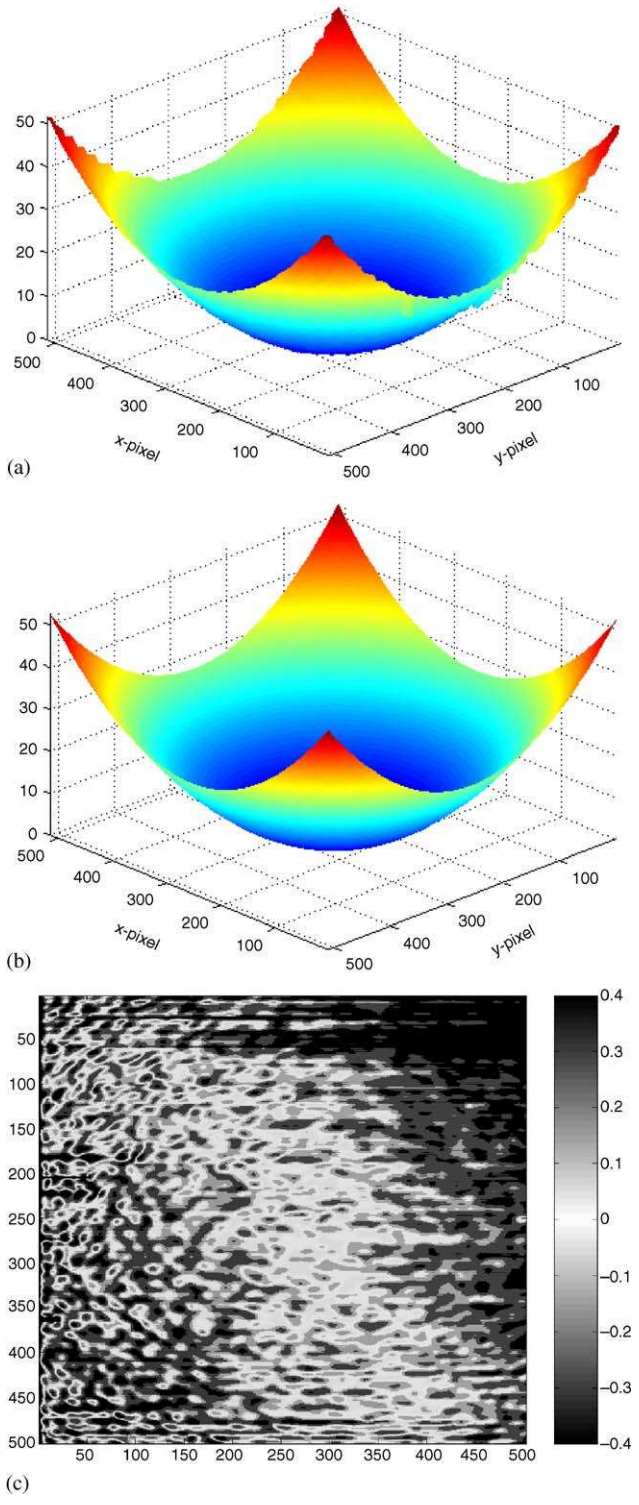

Fig. 6. (a) Retrieved phase distribution of the lower part of Fig. 6, (b) the exact phase distribution, (c) the difference between (a) and (b).

with high spatial frequency. The wavelet phase extraction algorithm was extended to DSPI. Its association with SWT denoising has provided a phase distribution with a good accuracy.

References

[1] Creath K. Phase-shifting speckle interferometry. Appl Opt 1985;24(18):3053–8.
[2] Nakadate S, Saito H. Fringe scanning speckle-pattern interferometry. Appl Opt 1985;24(18):2172–80.
[3] Mallat S. IEEE Trans Pattern Anal Mach Intell 1989;11(7):674.
[4] Pesquet JC, Krim H, Carfantan H. IEEE Trans Signal Process 1996;44(8):1964.
[5] Afifi M, Fassi-Fihri A, Marjane M, Nassim K, Sidki M, Rachafi S. Opt Commun 2002;211:47.
[6] Yura HT, Hanson SG. J Opt Soc Am A 1987;4:1931.
[7] Collins SA. J Opt Soc Am 1970;60:1168–77.
[8] Kogelnik H, Li T. Appl Opt 1966;5:1550.
[9] Goodman JW. In: Laser speckle and related phenomenon. Topics in applied physics, vol. 9. Berlin: Springer; 1975.
[10] de Lega XC. Processing of non-stationary interference patterns. Doctoral thesis, Ecole Polytechnique de Lausanne, 1997.
[11] Cherbuliez M, Jacquot P, de Lega XC. Wavelet processing of interferometric signals and fringe patterns. In: Wavelet applications in signal and image processing VII.
[12] Sciammarella CA, Kim T. Determination of strains from fringe patterns using space-frequency representations optical. Engineering 2003;42(11):3182.
[13] Sandoz P. Wavelet transform as a processing tool in white-light interferometry. Opt Lett 1997;22(14):1065–7.
[14] Sandoz P, Jacquot M. Signal processing of white light correlograms: simultaneous phase and envelope measurement by wavelet transformation, dans SPIE-Europto: optics for productivity in manufacturing, tome 3098. Munich, Allemagne; 1997. p. 73–82.
[15] Krüger S, Wernicke G, Osten W, Kayser D, Demoli N, Gruber H. Fault detection and feature analysis in interferometer fringe patterns by the application of wavelet filters in convolution processors. J Electron Imaging 2001;10:228–33.
[16] Berger E, von den Linden W, Dose V, Ruprecht MW, Koch AW. Approach for the evaluation of speckle deformation measurements by application of the wavelet transformation. Appl Opt 1997;36(29):7455–60.
[17] Federico A, Kaufmann GH, Serrano EP. Speckle noise reduction in ESPI fringes using wavelet shrinkage. In: Interferometry in speckle light: theory and applications. Berlin: Springer; 2000. p. 397–404.
[18] Federico A, Kaufmann GH. Phase retrieval in electronic speckle pattern interferometry using the continuous wavelet transform. Proceedings of the International Society for Optical Engineering, vol. 4419. 2001. p. 162–5.
[19] Federico A, Kaufmann GH. Comparative study of wavelet thresholding methods for denoising electronic speckle pattern interferometry fringes. Opt Eng 2001;40:2598–604.
[20] Federico A, Kaufmann GH. Evaluation of the continuous wavelet transform method for phase extraction in electronic speckle pattern interferometry. Opt Eng 2002;41:3209–16.
[21] Federico A, Kaufmann GH. Phase retrieval in digital speckle pattern interferometry using a chirped gaussian wavelet transform and a smoothed time-frequency distribution. Proceedings of the International Society for Optical Engineering, vol. 4933. 2003. p. 200–5.
[22] Daubachies I. Ten lectures on wavelets. Philadelphia: Society for industrial and Applied Mathematics; 1992.
[23] Mallat SG. A wavelet tour of signal processing 2nd ed. New York: Academic Press; 1999.
[24] Meyer Y. Wavelets: algorithms & applications. Philadelphia: Society for industrial and Applied Mathematics; 1993.
[25] Nason GP, Silverman BW. Lecture notes in statistics. Wavelets and statistics, vol. 103. New York: Springer; 1995. p. 281.
[26] Donoho DL, Johnstone IM. Adapting to unknown smoothness via wavelet shrinkage. Technical Report, Stanford University, 1992.